nature physics

Article

https://doi.org/10.1038/s41567-023-02177-2

Observation of the boson peak in a two-dimensional material

Received: 1 November 2022

Accepted: 18 July 2023

Published online: 4 September 2023

Check for updates

Martin Tømterud [1] ✉, Sabrina D. Eder [1], Christin Büchner [2,9], Lothar Wondraczek [3], Ingve Simonsen [4], Walter Schirmacher[5,6], Joseph R. Manson [7,8] & Bodil Holst [1] ✉

The boson peak is an excess in the phonon vibrational density of states relative to the Debye model. It has been observed in a wide range of amorphous materials, from inorganic glasses to polymers. Two-dimensional random matrix models and molecular dynamics simulations predict that the boson peak should also be present in amorphous two-dimensional materials, a notion that is of practical importance because it leads to an excess of heat capacity and influences transport properties. However, up until now, experimental observations in actual materials have not been possible due to the limited surface sensitivity of the methods usually applied to measure the boson peak. Here we present the experimental evidence of a boson peak in two-dimensional silica, through phonon spectra measured by means of inelastic helium-atom scattering. We identify the boson peak as a wavenumber-independent spectral maximum at a frequency similar to what has been observed in and predicted for bulk vitreous silica. Furthermore, we present a heterogeneous-elastic theory calculation in two dimensions, which shows how the vibrational coupling of the transversal and flexural shear vertical phonon modes produces the boson peak in two-dimensional materials at a frequency similar to that of the bulk, in agreement with our measurements.

The Debye model predicts that below the Debye frequency, the vibrational density of states for a solid material is proportional to ω^{D-1}, where D is the dimensionality and ω is the phonon frequency[1]. However, experiments have shown that many materials across the wide group of disordered materials exhibit a characteristic deviation from the Debye model prediction in the form of a broad, dispersionless excess of states relative to the expected frequency dependence. This deviation is commonly referred to as the boson peak (BP)[2–5]. The BP excess in the density of states is also found to be related to a similar excess in the heat capacity $C(T)$ measured at low temperatures. There, the BP appears as a hump in $C(T)/T^3$ in the bulk material at around 10 K (refs. 6,7). This hump in the heat capacity is associated with an opposite effect on the thermal conductivity. At the BP temperature, the thermal conductivity exhibits an upside-down BP[8]. This thermal anomaly is also associated with the BP[9]. The BP has furthermore been observed to influence energy transport in amorphous materials, where coexisting diffusive and propagative energy transport has been observed in the BP frequency range[10].

The BP has been observed using a wide range of measurement techniques: Raman spectroscopy[2,11–14]; optical spectroscopy[15] including

[1]Department of Physics and Technology, University of Bergen, Bergen, Norway. [2]Fritz-Haber-Institut der Max-Planck-Gesellschaft, Berlin, Germany. [3]Otto Schott Institute of Materials Research, University of Jena, Jena, Germany. [4]Department of Physics, NTNU–Norwegian University of Science and Technology, Trondheim, Norway. [5]Institute of Physics, University of Mainz, Mainz, Germany. [6]Center for Life Nano Science@Sapienza, Istituto Italiano di Tecnologia, Roma, Italy. [7]Department of Physics and Astronomy, Clemson University, Clemson, SC, USA. [8]Donostia International Physics Center (DIPC), Donostia-San Sebastián, Spain. [9]Present address: Lawrence Berkeley National Laboratory, Berkeley, CA, USA. ✉e-mail: martin.tomterud@uib.no; bodil.holst@uib.no

https://doi.org/10.1038/s41567-023-02177-2

far-infrared spectroscopy[16,17], X-rays[18], neutron scattering[19–21] and terahertz spectroscopy[22]; and thermal techniques[23] including indirect verification through measurements of the temperature dependence of heat capacity[8,24]. A BP-like anomaly in the vibrational density of states has also been observed in nanocrystalline ^{57}Fe (ref. 25), which is consistent with the results of simulations of nanocrystals[26]. Due to their limited surface sensitivity, all these experimental techniques address bulk material behaviour only; even grazing-incidence X-ray[27] and grazing-incidence neutron scattering[28] have penetration depths of a few nanometres, well above what one would consider the thickness of a two-dimensional (2D) material. Hence, the BP observed from such experiments reflects volumetric disorder. In three-dimensional (3D) vitreous silica, the BP has been reported by inelastic neutron[19] and inelastic X-ray scattering[14] near the frequency of ~6 meV, where the X-ray BP has much less intensity than the neutron one[14].

In 2007, the first observations of the BP as a surface phenomenon were obtained through the measurements of phonon dispersion curves on vitreous silica obtained using inelastic helium-atom scattering (HAS)[29–32]. HAS has a unique surface sensitivity. Unlike electrons, X-rays and neutrons (all of which interact with the core electronic cloud and atomic nuclei in the sample), the neutral helium atoms scatter off the outermost charge density distribution at the sample surface with no penetration into the bulk. The classical turning point for HAS at thermal energies is a few angstroms above the surface[33]. HAS is, therefore, particularly suited for this type of measurement[34].

The BP has been observed in 2D macroscopic model systems consisting of colloid particles[35] and photoelastic discs[36,37], and it was recently claimed to have been observed in ultrathin alumina layers on oxidized aluminium nanoparticles[38]; however, to date, it has not been experimentally observed in an atomically thin 2D material.

Theoretically, one has long assumed some form of disorder in a material to be a prerequisite for the existence of BP as a bulk phenomenon. Early approaches used soft potentials and double-well potentials introduced into the Hamiltonian[39–42]. The vibrational density of states for vitreous silica has been calculated using molecular dynamics simulations, leading to a prediction of the BP at around 6 meV (ref. 43) and around 7 meV (ref. 44), in good agreement with the experimental Raman scattering data[2]. Molecular dynamics simulations have also been used to calculate the BP at the surface of vitreous silica[45]. They obtained a BP at around 4 meV, in good agreement with the experimental HAS data mentioned above[29].

In 2004 (ref. 46) and later[9,47], it was shown that the origin of the BP in bulk glass can be explained in the framework of heterogeneous-elasticity theory (HET). In particular, the anomalies of specific heat and thermal conductivity in the ~10 K region were shown to have the same origin as the BP, namely, spatially fluctuating elastic constants.

At the same time, extensive simulations clarified that the BP-related vibrational anomalies of glasses are associated with non-affine displacement fields[48–52]. The non-affine aspects of the disorder-induced vibrational anomalies were shown to be accounted for by HET[47,53]. Further, the BP frequency was shown to coincide with the Ioffe–Regel limit for the existence of plane-wave-like states[47,54–56]. The states near and above the BP frequency were identified to be of the random matrix type[55,57,58].

The BP has been theoretically predicted to exist in 2D materials by molecular dynamics simulations[54] and random matrix models[59–61]. In a recent review of modern silicate glasses, the BP frequency of silica was reported using HET to vary between 4 and 6 meV (ref. 53).

In Methods, we present 2D HET calculations unpublished to date, to the best of our knowledge, which shows that the BP from elastic in-plane vibrations of a 2D material is coupled via disorder to the out-of-plane flexural shear vertical mode, also referred to as the ZA mode. This coupling arises via the disorder-induced frequency dependence of the effective flexural stiffness.

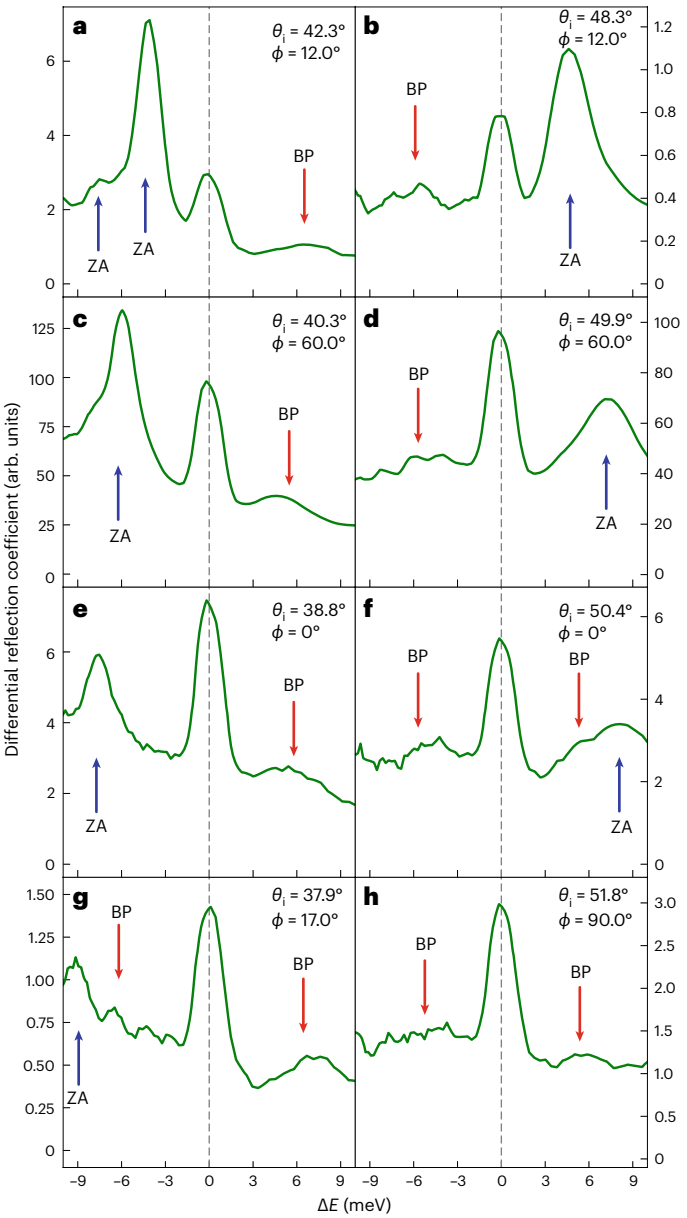

Fig. 1 | Several examples of HAS TOF spectra, converted to energy transfer Δ*E*, for 2D silica supported on Ru(0001). The incident polar angle relative to the sample normal is θ_i, and ϕ is the azimuthal angle of the sample relative to the principal axis of Ru(0001). The upward-pointing blue arrows indicate the ZA mode, and the downward-pointing red arrows indicate the BP.

In this paper, we present the first experimental observations of a BP in a 2D material: amorphous 2D silica supported on Ru(0001). This 2D film system has generated considerable interest because it is a transferable, wide-bandgap material. The 2D silica film is weakly bound to the Ru(0001) substrate and can be peeled off[62,63]. The silica bilayer is the thinnest arrangement of SiO_2 known[63] and—as it can be prepared in an amorphous phase—it has also been named the world's thinnest glass. The material is, therefore, of interest to the glass science community as it provides the opportunity to study a 2D glassy film and experimentally investigate how dimensionality impacts glassy properties. TEM imaging has been applied to confirm the 2D nature of the material[64] and to study atomic rearrangement in glass[65]. It has been shown[66] that the mechanical properties of free 2D silica can be extracted from the phonon frequency spectrum. As discussed in that work[66], the phonon spectrum exhibits no prominent features (except for the appearance of

https://doi.org/10.1038/s41567-023-02177-2

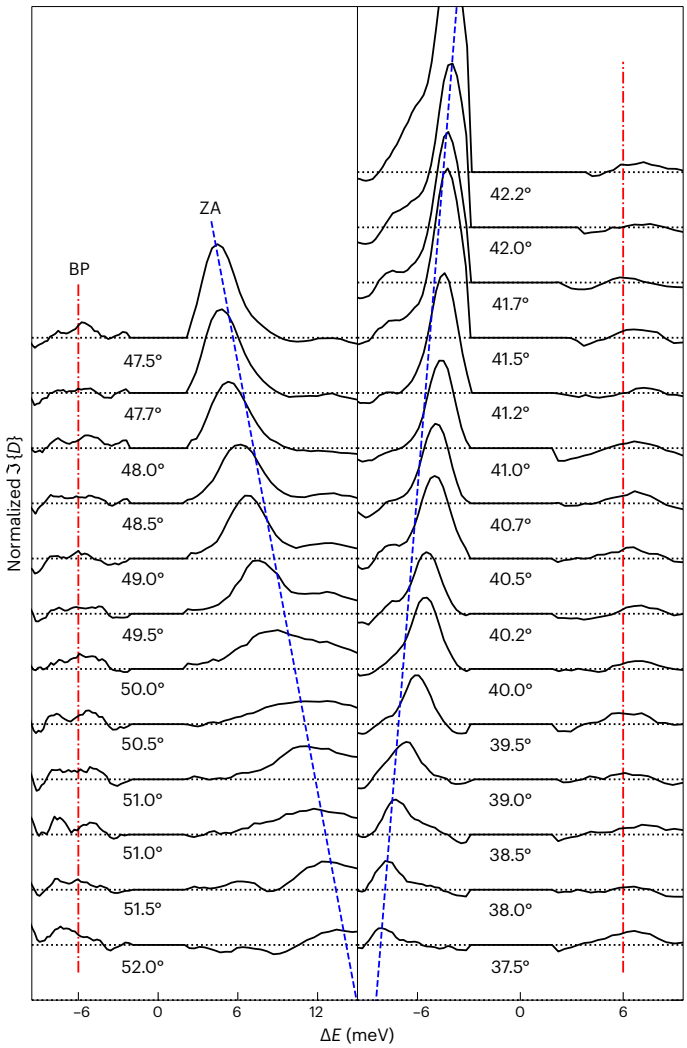

Fig. 2 | Spectral function normalized to a linear increase in ω as a function of ΔE. The individual spectra shown are a selection taken from the points shown in Fig. 4a, covering incident polar angles larger than specular (left side) and smaller than specular (right side). The region in the neighbourhood of the strong elastic peak at $\Delta E = 0$ has been subtracted away. The incident angles very close to specular at $\theta_i = 45°$ are not shown because the very intense ZA mode hides the BP. The blue dashed curve marks the dispersive ZA mode and the vertical red dash–dot lines mark the BP positions, which always remain at the same energy.

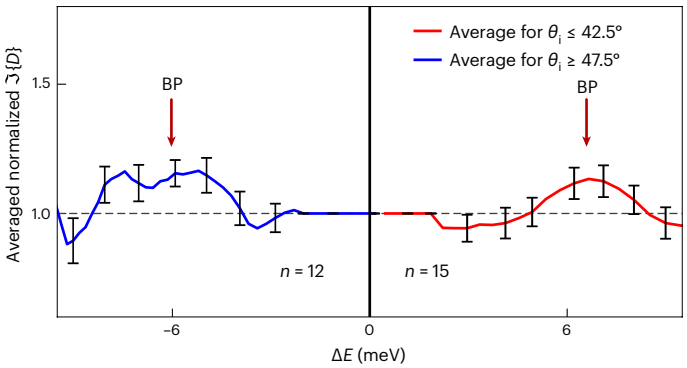

Fig. 3 | Average negative ΔE part of the spectral function. Average negative ΔE part of the spectral function in the left-hand column (left) and right-hand column (right) of Fig. 2. The error bars are one standard deviation of the average. The reference line at unity is drawn as a guide to the eye. The BP feature, indicated with arrow annotations, as well as its error bars are situated above the reference.

a gap in the dispersion of the ZA mode) that can be directly related to the underlying substrate. Therefore, this 2D film system provides an excellent framework for investigating the BP using HAS and comparing it with the aforementioned surface and bulk measurements. Because the BP is a disorder-induced phenomenon, the knowledge about this anomaly—and the corresponding modifications of the phonon spectrum—may be used for tuning the thermal properties of SiO_2 layers for applications[63]. Using inelastic HAS, we have obtained the time-of-flight (TOF) spectra that provide the basis of our experimental analysis. The experimental setup and methods are described in Methods. Examples of TOF spectra are shown converted to energy transfer ΔE (Fig. 1). These examples were chosen to cover the complete range of incident polar angles explored. The peak at $\Delta E = 0$ corresponds to diffuse elastic scattering, with no energy transfer with the surface. Negative values of ΔE correspond to phonon creation and positive values, to phonon annihilation. The upward-pointing arrows indicate the ZA mode, which were analysed in detail elsewhere[66] and used to obtain the bending rigidity of 2D silica. The downward-pointing arrows indicate the BP.

The TOF spectra, once they are converted to energy transfer, are known as the differential reflection coefficient $dR/d\Omega dE$: the number of helium atoms dR scattered within a small solid angle $d\Omega$ and small energy interval dE. In the HAS community, the differential reflection coefficient is usually expressed in terms of the surface phonon spectral density ρ_{zz} as[29,30]

$$\frac{dR}{d\Omega dE} \propto \frac{k_f}{|k_{i,z}|}|\tau_{fi}|^2|n(\omega)|e^{-2W(\mathbf{k}_f,\mathbf{k}_i,T)}(\Delta k_z)^2\rho_{zz}, \quad (1)$$

where we have introduced the momentum-transfer vector $\Delta\mathbf{k} = \mathbf{k}_f - \mathbf{k}_i$, and the indices i and f represent the states of the helium atom before and after the scattering event, respectively. The exponential is the Debye–Waller factor, and τ_{fi} is the form factor of the interaction potential between the helium atom and 2D silica. In the glass community, it is, however, more common to express the above equation in terms of the dynamical structure factor $S(\Delta\mathbf{k}, \omega)$. We, therefore, rewrite our equation as[67]

$$\frac{dR}{d\Omega dE} \propto \frac{k_f}{|k_{i,z}|}|\tau_{fi}|^2 S(\Delta\mathbf{k}, \omega). \quad (2)$$

The structure factor is proportional to the surface spectral function of 2D silica, $\mathfrak{I}D(\Delta\mathbf{k}, \omega)$ (appendix N in ref. 68), which, in turn, is equivalent to the spectral density $\rho_{zz} = \mathfrak{I}D(\Delta\mathbf{k}, \omega)$.

Figure 2 shows the examples of the spectral function spectra that have been normalized against the linear frequency dependence (see the 'Data analysis' section) and Fig. 3 shows the averages of these spectra.

The spectra are taken from points on the dispersion curves (Fig. 4a) for a sample azimuth of 12.0° relative to the high-symmetry direction of the Ru(0001) substrate and incident polar angles ranging from $\theta_i = 37.5°$ to 52.0°. In each spectrum shown in Fig. 2, the region close to the large elastic peak at $\Delta E = 0$ has been subtracted. The dashed blue curve marks the ZA mode. It disperses to higher-energy values as the incident angle moves further away from the specular position, corresponding to larger values of $|\Delta K|$. The BP appears at the same energy of about 6 meV (corresponding to mode annihilation; Fig. 2, right) and about −6 meV on the left (creation). The BP is denoted by a vertical red dash–dot line for all the conditions and has a full-width at half-maximum of about 3.5 meV. The averages in Fig. 3 (left) correspond to the negative-energy exchange region in Fig. 2 (left); similarly, the average on the positive-energy side in Fig. 3 corresponds to the positive-energy values in Fig. 2 (right). The error bars are taken to be one standard deviation. The error bars for BP are clearly situated above the reference line at unity. A HAS experiment measures only those inelastic

https://doi.org/10.1038/s41567-023-02177-2

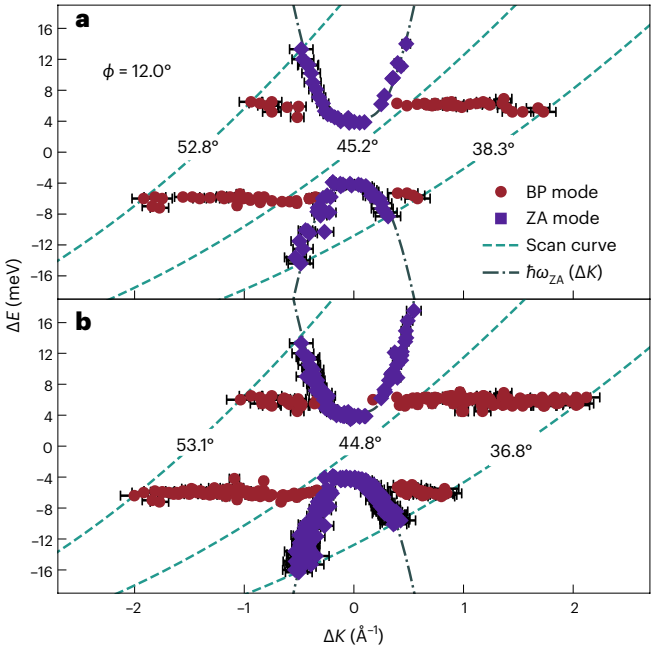

Fig. 4 | Phonon dispersion curves showing energy transfer ΔE as a function of parallel momentum transfer ΔK. a, Dispersion curve for all the polar angles θ_i measured at the single azimuthal angle $\phi = 12°$. The BP is shown as the red circle data points and the ZA mode as blue diamonds. The dotted green lines show the scan curves for three selected θ_i values, as indicated. **b**, Dispersion curves, including all the polar and azimuthal angles measured. The error bars are determined by the read-out limit resolution in ΔE and converted to ΔK.

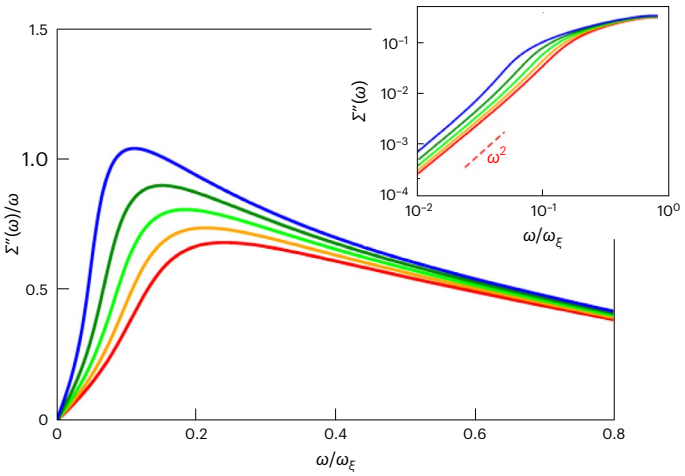

Fig. 5 | $\Sigma''(\omega)/\omega$ versus ω/ω_ξ. $\Sigma''(\omega)/\omega$ versus ω/ω_ξ with $\omega_\xi = [G_0/\rho_m]^{1/2} q_\xi$ and $\gamma = \langle(\Delta G)^2\rangle/G_0^2$ for $\gamma = 0.35$–0.39 (from bottom to top). The inset shows $\Sigma''(\omega)$ for the same parameters. The dashed line indicates the low-frequency ω^2 behaviour.

features that cross its scan curve, and this explains why the BP appears only at positive-energy transfer (Fig. 2, right).

Figure 4 shows the dispersion curves, that is, plots of ΔE as a function of parallel momentum transfer ΔK obtained as the maxima of $S(\Delta k, \omega)$, with $\omega = \Delta E/\hbar$. Figure 4a shows the measurements for all the polar angles taken at a single azimuthal angle of 12°, whereas Fig. 4b shows all the features observed at all the polar and azimuthal angles of the total 156 spectra datasets. Also, Fig. 4 shows three representative scan curves as dashed green curves denoted by the corresponding incident polar angle. The scan curves are obtained from the conservation of energy and parallel momentum for the largest and smallest incident angles measured, as well as the one closest to the specular position at $\theta_i = 45°$. The importance of the scan curves is that for a given θ_i, only those quantum features (inelastic or elastic) that the scan curves cross can be observed. The red circle data points give the positions of the BP mode in this figure, and it is clear that this is at very nearly constant energy for all the ΔK values, that is, it is dispersionless as expected[29]. In the vicinity of the ZA mode, the BP feature could not be distinguished because it is obscured by the much larger ZA peak.

In view of the mentioned simulational studies, which show irregular displacements and spatially fluctuating elastic constants associated with the BP anomaly[48,49,54–56,58–61], we can expect that in structurally disordered 2D systems, generically, a BP should be observed. This is in accordance with our 2D HET model (Methods and Fig. 5). Our model gives the important insight that the BP in a 2D material should occur at a similar frequency as in the bulk because the relevant elastic parameters of the 2D system should be similar to those in a 3D system.

Some scans (for example, Fig. 1 (top left)) contain a feature at about twice the energy of the BP with a full-width at half-maximum about twice as large. This feature could potentially be interpreted as a double excitation of the BP, if the BP itself is understood as a narrow collection of dispersionless modes. This will be a topic for further investigation.

To conclude, we present the first measurements of BP in a 2D material, namely, 2D silica. We obtain a value of around 6 meV (1.5 THz), in agreement with the BP position in bulk silica. We attribute our observation to in-plane elastic disorder, which couples to the low-frequency ZA mode probed through inelastic HAS. Future work should include (1) the measurements of 2D silica grown on other substrates[64] to assess the influence of the substrate binding energy on the BP behaviour; (2) temperature-dependent measurements to test if the blueshift behaviour observed for the surface BP of bulk silica also occurs in two dimensions; (3) measurements of the BP intensity in samples with different degrees of amorphicity, to investigate the possibility of 'tuning' the BP feature; and (4) further investigations of the potential double excitation of BP at higher energies and the consequences this observation would impose on the theory.

Online content

Any methods, additional references, Nature Portfolio reporting summaries, source data, extended data, supplementary information, acknowledgements, peer review information; details of author contributions and competing interests; and statements of data and code availability are available at https://doi.org/10.1038/s41567-023-02177-2.

References

1. Debye, P. Zur Theorie der spezifischen Wärme. *Ann. Phys.* **344**, 789–839 (1912).
2. Malinovsky, V. K. & Sokolov, A. P. The nature of boson peak in Raman scattering in glasses. *Solid State Commun.* **57**, 757–761 (1986).
3. Buchenau, U. et al. Low-frequency modes in vitreous silica. *Phys. Rev. B* **34**, 5665–5673 (1986).
4. Chumakov, A. I. et al. Collective nature of the boson peak and universal transboson dynamics of glasses. *Phys. Rev. Lett.* **92**, 245508 (2004).
5. Elliott, S. R. A unified model for the low-energy vibrational behaviour of amorphous solids. *Europhys. Lett.* **19**, 201 (1992).
6. Buchenau, U. Amorphous materials: low-frequency vibrations. in *Encyclopedia of Materials: Science and Technology* 212–215 (Elsevier, 2001).
7. Pohl, R. O. Amorphous materials: heat capacity. in *Encyclopedia of Materials: Science and Technology* 194–197 (Elsevier, 2001).
8. Zeller, R. C. & Pohl, R. O. Thermal conductivity and specific heat of noncrystalline solids. *Phys. Rev. B* **4**, 2029–2041 (1971).

9. Schirmacher, W. Thermal conductivity of glassy materials and the 'boson peak'. *Europhys. Lett.* **73**, 892–898 (2006).
10. Beltukov, Y. M., Parshin, D. A., Giordano, V. M. & Tanguy, A. Propagative and diffusive regimes of acoustic damping in bulk amorphous material. *Phys. Rev. E* **98**, 023005 (2018).
11. Jäckle, J. in *Amorphous Solids: Low-Temperature Properties* (ed Phillips, W. A.) 135 (Springer, 1981).
12. Duval, E., Boukenter, A. & Achibat, T. Vibrational dynamics and the structure of glasses. *J. Phys.: Condens. Matter* **2**, 10227 (1990).
13. Kabeya, M. et al. Boson peak dynamics of glassy glucose studied by integrated terahertz-band spectroscopy. *Phys. Rev. B* **94**, 224204 (2016).
14. Baldi, G., Giordano, V. M. & Monaco, G. Elastic anomalies at terahertz frequencies and excess density of vibrational states in silica glass. *Phys. Rev. B* **83**, 174203 (2011).
15. Schroeder, J., Lee, M., Saha, S. K. & Persans, P. D. Raman scattering in glasses at high temperature: the boson peak and structural relaxation kinetics in glasses. *J. Non-Cryst. Solids* **222**, 342–347 (1997).
16. Hutt, K. W., Phillips, W. A. & Butcher, R. J. Far-infrared properties of dilute hydroxyl groups in an amorphous silica matrix. *J. Phys.: Condens. Matter* **1**, 4767–4772 (1989).
17. Ohsaka, T. & Ihara, T. Far-infrared study of low-frequency vibrational states in As_2S_3 glass. *Phys. Rev. B* **50**, 9569–9572 (1994).
18. Benassi, P. et al. Evidence of high frequency propagating modes in vitreous silica. *Phys. Rev. Lett.* **77**, 3835–3838 (1996).
19. Buchenau, U., Nücker, N. & Dianoux, A. J. Neutron scattering study of the low-frequency vibrations in vitreous silica. *Phys. Rev. Lett.* **53**, 2316 (1984).
20. Wischnewski, A., Buchenau, U., Dianoux, A. J., Kamitakahara, W. A. & Zarestky, J. L. Neutron scattering analysis of low-frequency modes in silica. *Philos. Mag. B* **77**, 579–589 (1998).
21. Buchenau, U. Neutron scattering investigations of the boson peak. *Condens. Matter Phys.* **22**, 43601 (2019).
22. Mori, T. et al. Detection of boson peak and fractal dynamics of disordered systems using terahertz spectroscopy. *Phys. Rev. E* **102**, 022502 (2020).
23. Tomoshige, N., Mizuno, H., Mori, T., Kim, K. & Matubayasi, N. Boson peak, elasticity, and glass transition temperature in polymer glasses: effects of the rigidity of chain bending. *Sci. Rep.* **9**, 19514 (2019).
24. White, G. K., Collocott, S. J. & Cook, J. S. Thermal expansion and heat capacity of vitreous B_2O_3. *Phys. Rev. B* **29**, 4778–4781 (1984).
25. Fultz, B., Ahn, C. C., Alp, E. E., Stuhrhahn, W. & Toellner, T. S. Phonons in nanocrystalline ^{57}Fe. *Phys. Rev. Lett.* **79**, 937 (1997).
26. Kara, A. & Rahman, R. S. Vibrational properties of metallic nanocrystals. *Phys. Rev. Lett.* **81**, 1453 (1998).
27. Perlich, J. et al. Grazing incidence wide angle X-ray scattering at the wiggler beamline BW4 of HASYLAB. *Rev. Sci. Instrum.* **81**, 105105 (2010).
28. Müller-Buschbaum, P. Grazing incidence small-angle neutron scattering: challenges and possibilities. *Polym. J.* **45**, 34–42 (2012).
29. Steurer, W. et al. Observation of the boson peak at the surface of vitreous silica. *Phys. Rev. Lett.* **99**, 035503 (2007).
30. Steurer, W. et al. Surface dynamics measurements of silica glass. *Phys. Rev. B* **78**, 045427 (2008).
31. Steurer, W. et al. Anomalous phonon behavior: blueshift of the surface boson peak in silica glass with increasing temperature. *Phys. Rev. Lett.* **100**, 135504 (2008).
32. Steurer, W. et al. Vibrational excitations of glass observed using helium atom scattering. *J. Phys.: Condens. Matter* **20**, 224003 (2008).
33. Alderwick, A. R., Jardine, A. P., Allison, W. & Ellis, J. An evaluation of the kinematic approximation in helium atom scattering using wavepacket calculations. *Surf. Sci.* **678**, 65–71 (2018).
34. Holst, B. et al. Material properties particularly suited to be measured with helium scattering: selected examples from 2D materials, van der Waals heterostructures, glassy materials, catalytic substrates, topological insulators and superconducting radio frequency materials. *Phys. Chem. Chem. Phys.* **23**, 7653–7672 (2021).
35. Chen, K. et al. Low-frequency vibrations of soft colloidal glasses. *Phys. Rev. Lett.* **105**, 025501 (2010).
36. Zhang, L. et al. Experimental studies of vibrational modes in a two-dimensional amorphous solid. *Nat. Commun.* **8**, 67 (2017).
37. Wang, Y., Hong, L., Wang, Y., Schirmacher, W. & Zhang, J. Disentangling boson peaks and Van Hove singularities in a model glass. *Phys. Rev. B* **98**, 174207 (2018).
38. Cortie, D. L. et al. Boson peak in ultrathin alumina layers investigated with neutron spectroscopy. *Phys. Rev. Res.* **2**, 023320 (2020).
39. Karpov, V. G., Klinger, M. I. & Ignat'ev, F. N. Theory of the low-temperature anomalies in the thermal properties of amorphous structure. *Zh. Eksp. Teor. Fiz.* **84**, 775 (1983).
40. Buchenau, U., Galperin, Y. M., Gurevich, V. L. & Schober, H. R. Anharmonic potentials and vibrational localization in glasses. *Phys. Rev. B* **43**, 5039–5045 (1991).
41. Buchenau, U. et al. Interaction of soft modes and sound waves in glasses. *Phys. Rev. B* **46**, 2798–2808 (1992).
42. Parshin, D. A. Soft potential model and universal properties of glasses. *Phys. Scr.* **T49A**, 180–185 (1993).
43. Guillot, B. & Guissani, Y. Boson peak and high frequency modes in amorphous silica. *Phys. Rev. Lett.* **78**, 2401–2404 (1997).
44. Horbach, J., Kob, W. & Binder, K. High frequency sound and the boson peak in amorphous silica. *Eur. Phys. J. B* **19**, 531–543 (2001).
45. Wang, C., Tamai, Y. & Kuzuu, N. A molecular dynamics study on vibration spectra of a-SiO_2 surface. *J. Non-Cryst. Solids* **321**, 204–209 (2003).
46. Maurer, C. & Schirmacher, W. Local oscillators vs. elastic disorder: a comparison of two models for the boson peak. *J. Low-Temp. Phys.* **137**, 453–470 (2004).
47. Marruzzo, A., Schirmacher, W., Fratalocchi, A. & Ruocco, G. Heterogeneous shear elasticity of glasses: the origin of the boson peak. *Sci. Rep.* **3**, 1407 (2013).
48. Tanguy, A., Wittmer, J.-P. & Barrat, J.-L. Continuum limit of amorphous elastic bodies: a finite-size study of low-frequency harmonic vibrations. *Phys. Rev. B* **66**, 174205 (2002).
49. Maloney, C. & Lemaître, A. Universal breakdown of elasticity at the onset of material failure. *Phys. Rev. Lett.* **93**, 195501 (2004).
50. Léonforte, F., Tanguy, A., Wittmer, J. P. & Barrat, J.-L. Continuum limit of amorphous elastic bodies II: linear response to a point source force. *Phys. Rev. B* **70**, 014203 (2004).
51. Léonforte, F., Boissière, R., Tanguy, A., Wittmer, J. P. & Barrat, J.-L. Continuum limit of amorphous elastic bodies III: three-dimensional systems. *Phys. Rev. B* **72**, 224206 (2005).
52. Léonforte, F., Tanguy, A., Wittmer, J. P. & Barrat, J.-L. Inhomogeneous elastic response of silica glass. *Phys. Rev. Lett.* **97**, 055501 (2006).
53. Pan, Z. et al. Disorder classification of the vibrational spectra of modern glasses. *Phys. Rev. B* **104**, 134106 (2021).
54. Shintani, H. & Tanaka, H. Universal link between the boson peak and transverse phonons in glass. *Nat. Mater.* **7**, 870–877 (2008).
55. Beltukov, Y. M., Fusco, C., Parshin, D. A. & Tanguy, A. Theory of sparse random matrices and vibrational spectra of amorphous solids. *Phys. Rev. E* **93**, 023006 (2016).
56. Hu, Y.-C. & Tanaka, H. Origin of the boson peak in amorphous solids. *Nat. Phys.* **18**, 669–677 (2022).

57. Schirmacher, W., Diezemann, G. & Ganter, C. Harmonic vibrational excitations in disordered solids and the 'boson peak'. *Phys. Rev. Lett.* **81**, 136 (1998).
58. Beltukov, Y. M. & Parshin, D. A. Theory of sparse random matrices and vibrational spectra of amorphous solids. *Phys. Solid State* **53**, 151–162 (2011).
59. Conyuh, D. A., Beltukov, Y. M. & Parshin, D. A. Boson peak in two-dimensional random matrix models. *J. Phys. Conf. Ser.* **929**, 012031 (2017).
60. Conyuh, D. A. & Beltukov, Y. M. Random matrix theory and the boson peak in two-dimensional systems. *Phys. Solid State* **62**, 689–695 (2020).
61. Raikov, I. O., Conyuh, D. A., Ipatov, A. N. & Parshin, D. A. Boson peak in amorphous graphene in the stable random matrix model. *Phys. Solid State* **62**, 2143–2153 (2020).
62. Büchner, C. et al. A large-area transferable wide band gap 2D silicon dioxide layer. *ACS Nano* **10**, 7982–7989 (2016).
63. Büchner, C. & Heyde, M. Two-dimensional silica opens new perspectives. *Prog. Surf. Sci.* **92**, 341–374 (2017).
64. Huang, P. Y. et al. Direct imaging of a two-dimensional silica glass on graphene. *Nano Lett.* **12**, 1081–1086 (2012).
65. Huang, P. Y. et al. Imaging atomic rearrangements in two-dimensional silica glass: watching silica's dance. *Science* **342**, 224–227 (2013).
66. Büchner, C. et al. Bending rigidity of 2D silica. *Phys. Rev. Lett.* **120**, 226101 (2018).
67. Hofmann, F. & Toennies, J. P. High-resolution helium atom time-of-flight spectroscopy of low-frequency vibrations of adsorbates. *Chem. Rev.* **96**, 1307–1326 (1996).
68. Ashcroft, N. W. & Mermin, N. D. *Solid State Physics* (Harcourt College Publishers, 1976).

Methods

Experimental

The vitreous 2D silica sample was prepared in an ultrahigh vacuum on a Ru(0001) substrate at the Fritz Haber Institute, Berlin. We used the same sample that is described elsewhere[66]. After preparation, the sample was removed from the ultrahigh-vacuum chamber in Berlin and transported to Bergen. During transport, the sample was exposed to ambient conditions for more than 20 h. On arrival from Berlin, the sample was installed in the argon-vented sample chamber, which was then pumped down. The background pressure was around 1×10^{-9} mbar. A signal could be obtained from the sample without any initial cleaning; however, to ensure the maximum intensity before measurements were done, the sample was heated to 675 K for 1 h in an oxygen atmosphere ($p_{O_2} = 2.2 \times 10^{-6}$ mbar). This improved the measured signal. A slight decline in the reflected signal could be observed over a period of days. For this reason, the cleaning process was repeated every day before the measurements. This restored the original reflectivity. The HAS experiments were carried out in MAGIE, the molecular-beam apparatus at the University of Bergen[69,70]. The neutral helium beam was created by a free-jet expansion from a source reservoir through a 10.0 ± 0.5-μm-diameter nozzle. The central part of the beam was selected by a skimmer, 410 ± 2 μm in diameter, placed 17.0 ± 0.5 mm in front of the nozzle. All the experiments presented here were carried out on a room-temperature sample ($T = 296 \pm 1$ K). The source–detector scattering angle was held constant at 90°. The diffraction scans were measured with a room-temperature beam corresponding to a beam energy of $E_0 = 64$ meV, whereas for the TOF measurements, the beam was cooled to an energy of around $E_0 = 29$ meV. The stagnation pressure in the source reservoir was $p_0 = 81$ bar for all the TOF measurements. The incident-beam size was around 4 mm in diameter at the sample position. The TOF measurements were performed with a pseudorandom chopper[71]. The measurements presented were conducted as six independent series, varying the incident-beam angle (polar angle) θ_i at five different azimuthal angles, namely, $\phi \in \{0°, 12.0°, 17.0°, 60.0°, 90.0°\}$. In total, 156 TOF spectra were obtained. A low-energy electron diffraction analysis of the sample at the Fritz Haber Institute indicated that the sample was primarily vitreous. This is supported by the fact that no crystalline diffraction pattern was observed with HAS[66]. The azimuthal angle was varied to ensure that the effects measured were truly isotropic.

The thickness of an atomically thin layer is difficult to define, a problem well known in the study of single-layer graphene where it is called the Yakobson paradox[72]. Scanning tunnelling microscopy imaging has suggested a height of 3–5 Å for bilayer silica films on a Ru substrate[62,73]. Based on density functional theory calculations and the mechanical measurements of this sample presented in another work[66], this sample has been estimated to have a thickness of about 6.1 Å.

Data analysis

The dynamic structure factor $S(\Delta\mathbf{k}, \omega)$ for a solid with harmonic dynamics is given by

$$S(\Delta\mathbf{k}, \omega) = \mathrm{e}^{-2W(\mathbf{k}_f, \mathbf{k}_i, T)} \sum_{i=1}^{n} S^{(\nu)}(\Delta\mathbf{k}, \omega), \tag{3}$$

where the index ν in $S^{(\nu)}(\Delta\mathbf{k}, \omega)$ runs over the νth-phonon structure factors; one phonon, two phonon and so on. To get a good approximation, the structure factor of the inelastic HAS data is dominated by the one-phonon contribution. The one-phonon structure factor is by the fluctuation–dissipation theorem related to the strain–strain response function[74]

$$\begin{aligned} \chi(\Delta\mathbf{k}, \omega) &= \chi'(\Delta\mathbf{k}, \omega) + \mathrm{i}\chi''(\Delta\mathbf{k}, \omega) \\ &= (\Delta k)^2 D(\Delta\mathbf{k}, \omega), \end{aligned} \tag{4}$$

where $D(\Delta\mathbf{k},\omega) = D' + \mathrm{i}D''$ is the response function (Green's function) of the out-of-plane displacements. The dynamic structure factor is, therefore, given by

$$\begin{aligned} S^{(1)}(\Delta\mathbf{k}, \omega) &= |n(\omega)|\chi''(\Delta\mathbf{k}, \omega) \\ &= |n(\omega)|(\Delta k)^2 D''(\Delta\mathbf{k}, \omega) \end{aligned}. \tag{5}$$

Therefore, through the experimentally measured differential reflection coefficient, we have access to the imaginary part of Green's function, via

$$\frac{\mathrm{d}R}{\mathrm{d}\Omega \mathrm{d}E} \propto \frac{k_f}{|k_{i,z}|} |\tau_{fi}|^2 |n(\omega)| \mathrm{e}^{-2W(T)} (\Delta\mathbf{k})^2 D''(\Delta\mathbf{k}, \omega). \tag{6}$$

Rearranged, this gives

$$D''(\Delta\mathbf{k}, \omega) \propto \frac{\frac{\mathrm{d}R}{\mathrm{d}\Omega \mathrm{d}E} |k_{i,z}|}{k_f (\Delta\mathbf{k})^2 |n(\omega)| |\tau_{f,i}|^2 \exp[-2W(T)]}. \tag{7}$$

The Debye–Waller factor has been introduced as $\exp[-2W(\mathbf{k}_f, \mathbf{k}_i, T)]$ and the Bose–Einstein function as $n(\omega) = (\mathrm{e}^{\beta\hbar\omega} - 1)^{-1}$, where $\beta \equiv (k_B T)^{-1}$, k_B is Boltzmann's constant and T is the sample temperature. The absolute value sign around $n(\omega)$ signifies evaluating it as $n(\omega) + 1$ in creation events and $n(\omega)$ for annihilation events. The intensity of raw data is observed to linearly increase with ω, as expected for the background produced by the low-frequency acoustic phonon modes of a semi-infinite substrate, mediated by the electron density. We, therefore, present the normalized spectral function D'' as D''/ω.

The ZA mode of a thin film on a substrate has a well-understood dispersion relation given by[75]

$$\omega_{ZA}^2 = \frac{\kappa}{\rho_{2D}} (\Delta k)^4 + \omega_0^2, \tag{8}$$

where κ is the bending rigidity and ρ_{2D} is the 2D mass density. The gap, $\omega_0^2 = g/\rho_{2D}$, is proportional to the elastic-coupling strength between 2D silica and substrate, g (ref. 75). The form factor τ_{fi} is approximated using the well-known Morse potential matrix elements, that is, the distorted-wave matrix elements of the Morse potential taken with respect to its own eigenstates (chapter 8 in ref. 76). The argument of the Debye–Waller factor $2W(T)$ within the harmonic lattice approximation and for sufficiently large temperatures is linear in T. It is usually determined by measuring the temperature dependence of the specular diffraction peak. In the present set of experiments, the temperature dependence of the specular peak intensity was not measured; therefore, the argument was taken to be represented by $2W = (\Delta\mathbf{k}^2 C + D)T$, where the coefficients C and D were taken as fitting parameters. The coefficient D is proportional to the so-called Beeby correction, in which the attractive well depth of the interaction potential is added to the energy of normal motion of the helium atom[77]. As a check on this procedure, previous data from which the BP was determined at a silica surface[29] were re-examined using this method, and nearly identical results were found for both Debye–Waller factors and surface BP intensities.

Theoretical

2D HET. We consider a 2D system with spatially fluctuating shear modulus $G(\mathbf{r}) = G_0 + \Delta G(\mathbf{r})$, where G_0 is the mean and $\Delta G(\mathbf{r})$ are the fluctuations.

In two dimensions, longitudinal and transverse Green's functions (response functions of the in-plane displacements) are given by

$$D_{L,T}(q, \omega) = \frac{1}{-\omega^2 - \mathrm{i}\epsilon + q^2 v_{L,T}(\omega)^2} \tag{9}$$

As usual, one has to add an infinitely small positive real number to the spectral variable ω^2. The $v_{L,T}(\omega)$ values are effective, complex, frequency-dependent sound velocities, related to a complex, frequency-dependent shear modulus:

$$\begin{aligned}\rho_{2D} v_T(\omega)^2 &= G_0 - \Sigma(\omega) \equiv G(\omega),\\ \rho_{2D} v_L(\omega)^2 &= K + G(\omega),\end{aligned} \tag{10}$$

where K is the bulk modulus. In the self-consistent Born approximation, the equation for self-energy $\Sigma(\omega)$ is[9]

$$\Sigma(\omega) = \frac{1}{2}\gamma\left(\frac{1}{2\pi}\right)^2 \int_{|\mathbf{q}|<q_\xi} d^2q q^2 \left(D_L(q,\omega) + D_T(q,\omega)\right), \tag{11}$$

where $\gamma \propto \langle \Delta G^2 \rangle$ is the so-called disorder parameter. The upper cutoff q_ξ is inversely proportional to the correlation length ξ of the fluctuations. This equation predicts

$$\Sigma''(\omega) \propto \Gamma(\omega)/\omega \propto \omega^2, \text{ for } \omega < \omega_{BP}$$

where Γ is the the Brillouin linewidth and ω_{BP} is the BP frequency.

In Fig. 5, we have plotted $\Sigma''(\omega)/\omega$ versus ω; in this representation, the BP (which is actually a shoulder in the spectrum; inset) becomes visible.

Coupling to the out-of-plane vibrational degrees of freedom. The unperturbed Green function of the ZA modes is given by[75]

$$\begin{aligned}D^{(0)}_{ZA}(k,\omega) &= \frac{1}{-\omega^2 - i\epsilon + \omega^2_{ZA}(k)}\\ &= \frac{1}{-\omega^2 - i\epsilon + \omega_0^2 + \frac{1}{\rho_{2D}}\kappa k^4}\end{aligned}, \tag{12}$$

where $k \equiv |\Delta\mathbf{k}|$. The bending (flexural) rigidity κ is given by the layer thickness h, Poisson's ratio ν and Young's modulus of the three-dimensional material $Y_{3D} = 2G_{3D}(1+\nu)$ as

$$\kappa = \frac{h^3}{12(1-\nu^2)} Y_{3D} = \frac{h^3}{6(1-\nu)} G_{3D}. \tag{13}$$

Here G_{3D} is the 3D shear modulus, which obeys

$$G_{3D} = G_{2D}\frac{\rho_{3D}}{\rho_{2D}} = G_{2D}/h, \tag{14}$$

from which follows

$$\kappa = \frac{h^2}{6(1-\nu)} G_{2D}. \tag{15}$$

This establishes the coupling of the ZA mode to the 2D shear elasticity. In the model of 2D heterogeneous elasticity introduced earlier, the BP is produced by the frequency dependence of the 2D shear modulus $G(\omega)$. This will give rise to a corresponding frequency dependence of the bending rigidity of the ZA modes, that is, we have to replace the 2D shear modulus in equation (15) by the frequency-dependent one given by equation (10). The effective complex and frequency-dependent flexural stiffness, which provides the coupling of the ZA modes to the in-plane BP, is given by

$$\kappa(\omega) = \frac{h^2}{6(1-\nu)} G_{2D}(\omega) = \frac{h^2}{6(1-\nu)} \left(G_0 - \Sigma(\omega)\right), \tag{16}$$

so that we may write

$$D_{ZA}(k,\omega) = \frac{1}{-\omega^2 + i\epsilon + \omega^2_{ZA}(k) - \Pi(k,\omega)} \tag{17}$$

with

$$\Pi(k,\omega) = V(k)\Sigma(\omega) \tag{18}$$

and the vertex function

$$V(k) = \frac{1}{G_0}\left(\omega^2_{ZA}(k) - \omega_0^2\right). \tag{19}$$

In other words, the in-plane disorder-induced anomalous elasticity—with its 2D BP—is coupled to the flexural out-of-plane degrees of freedom in the same way as the shear modulus to bending rigidity[75].

For the spectral function, we finally get

$$\chi''(k,\omega) \propto \frac{k^2 V(k)\Sigma''(\omega)}{\left[\omega^2_{ZA}(k) - \Pi'(k,\omega)\right]^2 + \Pi''(k,\omega)^2}. \tag{20}$$

The spectral function is proportional to $\Sigma''(\omega)$, that is, the spectral function, divided by ω, exhibits a BP (Fig. 5).

Data availability

The experimental dataset is available via DataverseNO at https://doi.org/10.18710/CMKTQX (ref. 78).

References

69. Apfolter, A. *Wiederaufbau und Test einer He-Streuapparatur und erste Streuexperimente an amorpher sowie kristalliner SiO_2 Oberfläche*. Master's thesis, Graz University of Technology (2005).
70. Eder, S. D., Samelin, B., Bracco, G., Ansperger, K. & Holst, B. A free jet (supersonic), molecular beam source with automatized, 50 nm precision nozzle-skimmer positioning. *Rev. Sci. Instrum.* **84**, 093303 (2013).
71. Koleske, D. D. & Sibener, S. J. Generation of pseudorandom sequences for use in cross-correlation modulation. *Rev. Sci. Instrum.* **63**, 3852–3855 (1992).
72. Huang, Y., Wu, J. & Hwang, K. C. Thickness of graphene and single-wall carbon nanotubes. *Phys. Rev. B* **74**, 245413 (2006).
73. Yang, B. et al. Thin silica films on Ru(0001): monolayer, bilayer and three-dimensional networks of [SiO_4] tetrahedra. *Phys. Chem. Chem. Phys.* **14**, 11344–11351 (2012).
74. Schirmacher, W., Scopigno, T. & Ruocco, G. Theory of vibrational anomalies in glasses. *J. Non-Cryst. Solids* **407**, 133–140 (2015).
75. Amorim, B. & Guinea, F. Flexural mode of graphene on a substrate. *Phys. Rev. B* **88**, 115418 (2013).
76. Goodman, F. O. & Wachman, H. Y. Quantum theory of gas-surface scattering. in *Dynamics of Gas-Surface Scattering* 143–180 (Elsevier, 1976).
77. Beeby, J. L. The scattering of helium atoms from surfaces. *J. Phys. C: Solid State Phys.* **4**, 359–362 (1971).
78. Holst, B., Eder, S. D. & Tømterud, M. Helium atom scattering on amorphous bilayer silica; https://doi.org/10.18710/CMKTQX

Acknowledgements

We want to specially thank H.-J. Freund and M. Heyde for making the 2D silica sample available for these experiments. We also thank W. Steurer for useful discussions and acknowledge the valuable contributions and stimulating discussions with G. Pacchioni. L.W. acknowledges funding from the Carl Zeiss Foundation through its breakthrough program. B.H. acknowledges funding from the Research Council of Norway (project nos. 213453 and 234159), both within the FRIPRO program. M.T. acknowledges funding from the Research Council of Norway (project no. 337339) (travel support).

Author contributions

C.B. prepared the sample, S.D.E. performed the experiments and M.T. performed the data analysis. L.W. and W.S. provided the theoretical model. I.S. and J.R.M. supported the analysis. B.H. designed the experiments. M.T., J.R.M. and B.H. wrote the paper with contributions from all authors.

Competing interests

The authors declare no competing interests.

Additional information

Correspondence and requests for materials should be addressed to Martin Tømterud or Bodil Holst.

Peer review information *Nature Physics* thanks Anne Tanguy, Talat Rahman and Hideyuki Mizuno for their contribution to the peer review of this work.